Efficient vector radiative transfer calculations in vertically inhomogeneous cloudy atmospheres

Bastiaan van Diedenhoven, Otto P. Hasekamp, and Jochen Landgraf

Accurate radiative transfer calculations in cloudy atmospheres are generally time consuming, limiting their practical use in satellite remote sensing applications. We present a model to efficiently calculate the radiative transfer of polarized light in atmospheres that contain homogeneous cloud layers. This model combines the Gauss–Seidel method, which is efficient for inhomogeneous cloudless atmospheres, with the doubling method, which is efficient for homogeneous cloud layers. Additionally to reduce the computational effort for radiative transfer calculations in absorption bands, the cloud reflection and transmission matrices are interpolated over the absorption and scattering optical thicknesses within the cloud layer. We demonstrate that the proposed radiative transfer model in combination with this interpolation technique is efficient for the simulation of satellite measurements for inhomogeneous atmospheres containing one homogeneous cloud layer. For example, the Scanning Imaging Absorption Spectrometer for Atmospheric Cartography (SCIAMACHY) measurements in the oxygen A band (758–773 nm) and the Hartley–Huggins ozone band (295–335 nm) with a spectral resolution of 0.4 nm can be simulated for these atmospheres within 1 min on a 2.8 GHz PC with an accuracy better than 0.1%. © 2006 Optical Society of America

OCIS codes: 290.1090, 280.1310, 010.1310, 290.1350.

1. Introduction

Satellite measurements of reflected sunlight in the ultraviolet (UV), visible, and short-wave infrared play an important role in monitoring the atmospheric composition. For example, measurements of the Global Ozone Monitoring Experiment (GOME),[1] the Scanning Imaging Absorption Spectrometer for Atmospheric Cartography (SCIAMACHY),[2] and the Ozone Monitoring Instrument (OMI),[3] are used to monitor ozone, nitrogen dioxide (NO_2), sulphur dioxide (SO_2), water vapor, aerosols, and other atmospheric compounds. Due to the large field of view of many of these satellite instruments, clouds influence most of their measurements. For example, the fields of view of the GOME (320 km $\times$ 40 km), the SCIAMACHY (60 km $\times$ 40 km), and the OMI (13 km $\times$ 24 km) imply that, on average, about 99%, 95%, and 92% of their measurements, respectively, are contaminated by clouds.[4] Clouds can have a big effect on the retrieval of trace gas amounts.[5,6] Therefore algorithms for the interpretation of these satellite measurements should take the effect of clouds into account. However, accurate radiative transfer calculations in cloudy atmospheres are generally time consuming. To overcome this, often simple approximations are used to describe clouds in retrieval algorithms. The most widely used approximation is the description of clouds as reflecting and absorbing surfaces that do not transmit radiation.[7,8] Moreover, the cloud reflection is often assumed to be Lambertian.[9]

Recent studies have shown that this approximative treatment of clouds can cause substantial errors in the retrieval products from satellites.[10,11] For instance, Liu *et al.*[10] showed that not accounting for ozone absorption within a cloud can result in errors in the total ozone amounts of approximately 1%–10%. Moreover, they showed that these errors greatly depend on viewing and illumination geometry and the amount and distribution of ozone within the cloud. Also in retrievals of cloud properties using absorption bands of oxygen,[9,12,13] neglecting the enhancement of absorption inside the clouds leads to an underestimation of the cloud top height.[7,14] In addition, the coupling between scattering on cloud particles and molecular Rayleigh scattering needs to be taken into account, especially in the UV.[11,15] Thus a radiative

The authors are with the SRON Netherlands Institute for Space Research, Sorbonnelaan 2, 3584 CA Utrecht, The Netherlands. B. van Diedenhoven's e-mail address is b.van.diedenhoven@sron.nl.

Received 4 January 2006; accepted 17 February 2006; posted 16 March 2006 (Doc. ID 66898).

0003-6935/06/235993-14$15.00/0

© 2006 Optical Society of America

transfer model used for the interpretation of satellite measurements of cloudy atmospheres should take scattering and absorption inside clouds into account.

Additionally, such a radiative transfer model should take polarization into account. Namely, clouds can polarize incoming solar radiation or depolarize radiation that has been scattered by molecules and/or aerosols, depending on the scattering geometry.[16–19] These polarization effects should be taken into account to model the radiance correctly and correctly model measurements of polarization-sensitive instruments such as the GOME and the SCIAMACHY.[18] Furthermore, satellite measurements of the state of polarization, as performed, e.g., by the Polarization and Directionality of the Earth's Reflectances (POLDER) and Polarization and Anisotropy of Reflectances for Atmospheric Sciences Coupled with Observations from a Lidar (PARASOL) instruments[20] and the Aerosol Polarimetry Sensor (APS) instrument, scheduled to fly on the NASA Glory Mission,[21] contain important information on, e.g., cloud optical thickness and size distribution.[16,18,19,21,22] Obviously, extraction of this information requires a radiative transfer model including polarization.

Current (vector) radiative transfer codes, based on, e.g., the doubling–adding,[23] Gauss–Seidel,[24] and discrete ordinate[25] techniques are generally time consuming for inhomogeneous atmospheres that contain clouds. The efficient approximative treatment of cloud layers using asymptotic relations as described by Kokhanovsky[26] can include reflection and transmission of polarized light. However, these relations are only accurate for weakly absorbing media with a scattering optical thickness larger than 5 and can yield large errors when used in wavelength windows including strong absorption bands.[27]

The aim of this paper is to present a radiative transfer model that is sufficiently efficient to be practically used in retrieval applications. For these applications, radiative transfer calculations have to be performed for atmospheres that contain a limited number of homogeneous cloud layers (in most cases one cloud layer), whereas the rest of the atmosphere is described by homogeneous layers containing molecules and/or aerosols with a much smaller scattering optical thickness. The radiative transfer problem for such a model atmosphere can be solved in two steps. First, the radiative transfer equation is solved for each individual layer. For this step, we use the layer average intensity approximation for noncloudy layers and the doubling method[23] for cloud layers. Second, the boundary conditions at the layer interfaces are matched, which results in a matrix equation with respect to the corresponding intensity vectors. In the presented model, this equation is efficiently solved using the Gauss–Seidel iteration method. The efficiency of this Combined Doubling and Gauss–Seidel (CODAGS) model is demonstrated by a comparison to the doubling–adding approach. Furthermore, we show how the number of Gaussian-quadrature streams in the optically thin atmospheric layers can be reduced with respect to those used in the cloud layer, significantly reducing the calculation time.

For most retrieval applications, radiative transfer calculations have to be performed at many wavelengths in an atmospheric absorption band. To optimize CODAGS for absorption bands, we significantly reduce the number of calculations for the cloud layer, which is by far the most time-consuming part of CODAGS. The number of cloud calculations is reduced by interpolating the cloud reflection and transmission matrices over the scattering and absorption optical thicknesses within the cloud layer. The required accuracy of the Stokes parameters at the top of atmosphere can be specified beforehand. The accuracy and efficiency of this technique are demonstrated by its application on the radiative transfer calculations in the oxygen A band in the near-infrared and the Hartley–Huggins ozone absorption band in the UV.

The paper is constructed as follows. In Section 2 we discuss the theoretical background of the CODAGS model. The computational effort and accuracy of this model are discussed in Section 3. In Section 4, the reduction of Gaussian-quadrature streams is discussed. Next, in Section 5, we present the interpolation technique for spectral windows including absorption bands. In Section 6, the practical application of the presented radiative transfer model is demonstrated by accurately simulating the SCIAMACHY measurements. Finally, we conclude the paper in Section 7.

2. Theory

A. Radiative Transfer Problem in Matrix Form

The radiance and the polarization of radiation can be described by an intensity vector $\mathbf{I}$, which has the Stokes parameters I, Q, U, and V as its components,[28,29] i.e.,

$$\mathbf{I} = [I,\ Q,\ U,\ V]^T, \tag{1}$$

where T indicates the transposed vector. We define $\mathbf{I}$ relative to the local meridian plane.

In this section, a general solution for the radiative transfer problem for diffuse light is discussed. The directional zenith dependence of the intensity field $\mathbf{I}$ is described by N Gaussian-quadrature streams and the azimuthal dependence by a Fourier series, as proposed by Hovenier and van der Mee[29] (see Appendix A).

Let us consider a plane-parallel, vertically inhomogeneous atmosphere containing M homogeneous model layers. For several methods to solve the radiative transfer problem in a homogeneous model layer k, ranging from optical depth τ_{k-1} to τ_k, the outgoing upward intensity at the upper layer boundary is subject to a set of linear equations of the type

$$\begin{aligned}\mathbf{I}^m(\tau_{k-1},\ \mu_i) = \sum_{j=-N}^{N} a_j\big[&\boldsymbol{\alpha}_k^m(\mu_j,\ \mu_i)\mathbf{I}^m(\tau_{k-1},\ \mu_j)\\ &+ \boldsymbol{\beta}_k^m(\mu_j,\ \mu_i)\mathbf{I}^m(\tau_k,\ \mu_j)\big]\\ &+ \boldsymbol{\gamma}_k^m(\mu_i)\mathbf{F}_0 \exp(-\tau_k/\mu_0),\end{aligned} \tag{2}$$

for each Fourier term m and Gaussian-quadrature angle μ_i (with $i < 0$ for the downward directions and $i > 0$ for the upward directions). Here a_j are the Gaussian-quadrature weights. The vector $\mathbf{F}_0$ is defined by $\mathbf{F}_0 = [F_0, 0, 0, 0]^T$, where F_0 is the solar incident flux per unit area perpendicular to the solar beam in the direction μ_0. A similar equation holds for the downward intensity at the lower layer boundary. Expressions for the 4×4 matrices $\boldsymbol{\alpha}_k^m$ and $\boldsymbol{\beta}_k^m$ and the four-dimensional vector $\boldsymbol{\gamma}_k^m$ depend on the chosen radiative transfer solution technique.

Matching the continuity conditions at the layer boundaries, we obtain

$$\boldsymbol{\Phi}_+^{k-1} = \mathbf{A}_{++}^k \boldsymbol{\Phi}_+^{k-1} + \mathbf{A}_{+-}^k \boldsymbol{\Phi}_-^{k-1} + \mathbf{B}_{++}^k \boldsymbol{\Phi}_+^k + \mathbf{B}_{+-}^k \boldsymbol{\Phi}_-^k + \boldsymbol{\Gamma}_+^k \mathbf{F}_0 \exp(-\tau_{k-1}/\mu_0), \tag{3}$$

$$\boldsymbol{\Phi}_-^k = \mathbf{A}_{-+}^k \boldsymbol{\Phi}_+^k + \mathbf{A}_{--}^k \boldsymbol{\Phi}_-^k + \mathbf{B}_{-+}^k \boldsymbol{\Phi}_+^{k-1} + \mathbf{B}_{--}^k \boldsymbol{\Phi}_-^{k-1} + \boldsymbol{\Gamma}_-^k \mathbf{F}_0 \exp(-\tau_{k-1}/\mu_0) \tag{4}$$

for $k = 1, \ldots, M$. The $4N$-dimensional vectors are defined by

$$\boldsymbol{\Phi}_\pm^k = \begin{bmatrix} \mathbf{I}^m(\tau_k, \mu_{\pm 1}) \\ \vdots \\ \mathbf{I}^m(\tau_k, \mu_{\pm N}) \end{bmatrix}, \quad \Gamma_\pm^k = \begin{bmatrix} \boldsymbol{\gamma}_k^m(\mu_{\pm 1}) \\ \vdots \\ \boldsymbol{\gamma}_k^m(\boldsymbol{\mu}_{\pm N}) \end{bmatrix}. \tag{5}$$

Furthermore, the $4N \times 4N$ matrices $\mathbf{A}_{++}^k$ and $\mathbf{B}_{\pm\pm}^k$ in Eqs. (3) and (4) are given by

$$\begin{aligned} \mathbf{A}_{\pm\pm}^k &= \left[\boldsymbol{\alpha}_k^m(\mu_{\pm j}, \mu_{\pm i})\right], \\ \mathbf{B}_{\pm\pm}^k &= \left[\boldsymbol{\beta}_k^m(\mu_{\pm j}, \mu_{\pm i})\right], \end{aligned} \tag{6}$$

with $i, j = 1, \ldots, N$. The vector $\boldsymbol{\Phi}$ is subject to the boundary conditions

$$\boldsymbol{\Phi}_-^0 = [0, \ 0, \ 0, \ 0]^T, \tag{7}$$

$$\boldsymbol{\Phi}_+^M = \mathbf{A}_S \boldsymbol{\Phi}_-^M + \boldsymbol{\Gamma}_S \mathbf{F}_0 \exp(-\tau_M/\mu_0), \tag{8}$$

where the $4N \times 4N$ matrix $\mathbf{A}_S$ is given by

$$\mathbf{A}_S = \left[\boldsymbol{\alpha}_S^m(\mu_{-j}, \mu_i)\right], \tag{9}$$

with the 4×4 submatrices

$$\boldsymbol{\alpha}_S^m(\mu_{-j}, \mu_i) = 2\mu_j \mathbf{R}_S^m(\mu_j, \mu_i), \tag{10}$$

with $i, j = 1, \ldots, N$, and where $\mathbf{R}_S^m$ is the mth Fourier term of the bidirectional reflection distribution matrix of the surface. The $4N$-dimensional vector $\boldsymbol{\Gamma}_S$ has the coefficients

$$\boldsymbol{\gamma}_S^m(\mu_i) = \frac{\mu_0}{\pi} \mathbf{R}_S^m(\mu_0, \mu_i), \tag{11}$$

with $i = 1, \ldots, N$. For the whole model atmosphere, Eqs. (3), (4), (7), and (8) can be summarized in the matrix equation

$$\mathbf{M}\boldsymbol{\Phi} = \mathbf{C}, \tag{12}$$

with the $(2M + 1)4N$-dimensional vectors

$$\boldsymbol{\Phi} = \begin{bmatrix} \boldsymbol{\Phi}_+^0 \\ \boldsymbol{\Phi}_-^1 \\ \boldsymbol{\Phi}_+^1 \\ \boldsymbol{\Phi}_-^2 \\ \boldsymbol{\Phi}_+^2 \\ \vdots \\ \boldsymbol{\Phi}_+^{M+1} \\ \boldsymbol{\Phi}_-^M \\ \boldsymbol{\Phi}_+^M \end{bmatrix}, \quad \mathbf{C} = \begin{bmatrix} \boldsymbol{\Gamma}_+^1 \\ \boldsymbol{\Gamma}_-^1 \\ \boldsymbol{\Gamma}_+^2 \\ \Gamma_-^2 \\ \vdots \\ \boldsymbol{\Gamma}_+^M \\ \boldsymbol{\Gamma}_-^M \\ \boldsymbol{\Gamma}_S \end{bmatrix}, \tag{13}$$

and the $(2M + 1)4N \times (2M + 1)4N$ sparse matrix

$$\mathbf{M} = \mathbf{1} - \begin{bmatrix} \mathbf{A}_{++}^1 & \mathbf{B}_{+-}^1 & \mathbf{B}_{++}^1 & 0 & \cdots & & & & \cdots & 0 \\ \mathbf{B}_{-+}^1 & \mathbf{A}_{--}^1 & \mathbf{A}_{-+}^1 & 0 & \cdots & & & & \cdots & 0 \\ 0 & \mathbf{A}_{+-}^2 & \mathbf{A}_{++}^2 & \mathbf{B}_{+-}^2 & \mathbf{B}_{++}^2 & 0 & \cdots & & \cdots & 0 \\ 0 & \mathbf{B}_{--}^2 & \mathbf{B}_{-+}^2 & \mathbf{A}_{--}^2 & \mathbf{A}_{-+}^2 & 0 & \cdots & & \cdots & 0 \\ \vdots & \cdots & & & & \ddots & & & & \vdots \\ 0 & \cdots & & & \cdots & 0 & \mathbf{A}_{+-}^M & \mathbf{A}_{++}^M & \mathbf{B}_{+-}^M & \mathbf{B}_{++}^M \\ 0 & \cdots & & & \cdots & 0 & \mathbf{B}_{--}^M & \mathbf{B}_{-+}^M & \mathbf{A}_{--}^M & \mathbf{A}_{-+}^M \\ 0 & \cdots & & & & & \cdots & 0 & \mathbf{A}_S & 0 \end{bmatrix}, \tag{14}$$

where $\mathbf{1}$ is the corresponding unity matrix. Hence for known coefficients $\boldsymbol{\alpha}_k^m$, $\boldsymbol{\beta}_k^m$, and $\boldsymbol{\gamma}_k^m$, the diffuse intensity vector field at the layer boundaries is found from the solution of matrix equation (12). For this purpose, several techniques exist (see, e.g., Press *et al.*[30]), of which the Gauss–Seidel and the lower-triangular–

upper-triangular (LU) decomposition techniques are the most widely used. An efficient variant of the Gauss–Seidel technique was first proposed by Herman and Browning[31] and worked out thoroughly by Landgraf *et al.*[32] In Subsections 2.B and 2.C we discuss the use of the layer average intensity approximation method and the doubling method to obtain $\boldsymbol{\alpha}_k^m$, $\boldsymbol{\beta}_k^m$, and $\boldsymbol{\gamma}_k^m$ for an atmosphere that contains clouds.

B. Layer Average Intensity Approximation for Optically Thin Layers

To obtain expressions for $\boldsymbol{\alpha}_k^m$, $\boldsymbol{\beta}_k^m$, and $\boldsymbol{\gamma}_k^m$, a common approach in radiative transfer models employing the Gauss–Seidel technique is to approximate the intensities by their layer average, i.e.,

$$\bar{\mathbf{I}}^m(\mu_i) = \frac{1}{2}\left[\mathbf{I}^m(\tau_{l-1},\ \mu_i) + \mathbf{I}^m(\tau_l,\ \mu_i)\right] \quad \text{for } \tau_{l-1} < \tau < \tau_l \tag{15}$$

for $i = -N, \ldots, -1, 1, \ldots, N$. Following Hasekamp,[33] $\boldsymbol{\alpha}_k^m$ and $\boldsymbol{\beta}_k^m$ are then defined by

$$\boldsymbol{\alpha}_k^m(\mu_{\pm j},\ \mu_{\pm i}) = \frac{\omega_k}{4}\mathbf{Z}_k^m(\mu_{\pm j},\ \mu_{\pm i})[1 - \exp(-\Delta\tau_k/\mu_i)],$$

$$\boldsymbol{\beta}_k^m(\mu_{\pm j},\ \mu_{\pm i}) = \boldsymbol{\alpha}_k^m(\mu_{\pm j},\ \mu_{\pm i}) + \delta_{ij}\exp(-\Delta\tau_k/\mu_i\mathbf{E}), \tag{16}$$

and $\boldsymbol{\gamma}_k^m$ is defined by

$$\boldsymbol{\gamma}_k^m(\mu_{\pm i}) = \frac{\omega_k}{4\pi}\frac{\mu_o}{\mu_o + \mu_i}\mathbf{Z}_k^m(-\mu_o,\ \mu_{\pm i}), \tag{17}$$

with $i, j = 1, \ldots, N$. Here, ω_k is the single-scattering albedo, $\mathbf{E}$ is the 4×4 unity matrix, and δ_{ij} is the Kronecker delta. Furthermore, $\mathbf{Z}_k^m$ is the mth Fourier term of the scattering phase matrix, which can be calculated by

$$\mathbf{Z}_k^m(\mu_j,\ \mu_i) = (-1)^m\sum_{l=m}^{\infty}\mathbf{P}_m^l(-\mu_i)\mathbf{S}_k^l\mathbf{P}_m^l(-\mu_j), \tag{18}$$

where $\mathbf{S}_k^l$ is the expansion coefficient matrix, and $\mathbf{P}_m^l$ is the generalized spherical function matrix.[23,29]

Thus the layer average intensity approximation of Eq. (15) allows the coefficients $\boldsymbol{\alpha}_k^m$, $\boldsymbol{\beta}_k^m$, and $\boldsymbol{\gamma}_k^m$ to be expressed directly in terms of the scattering phase function and the single-scattering albedo. The layer average intensity approximation is valid for optically thin layers. To limit the errors caused by Eq. (15), the model layers are split into thin sublayers, such that their scattering and absorption optical thicknesses do not exceed the thresholds Δ_{scat} and Δ_{abs}, respectively. The layer splitting procedure is discussed by Landgraf *et al.*[32]

The layer average intensity approximation method is efficient for solving the radiative transfer in clear-sky atmospheres, including Rayleigh scattering, as well as in atmospheres including additional aerosols, as shown by Hasekamp and Landgraf.[24] However, as noted before by Hansen[34] and Herman *et al.*,[35] among others, the method becomes relatively time consuming when considering atmospheres with a large scattering optical thickness, such as atmospheres containing clouds. This is illustrated in Fig. 1, where the computation time is shown for the radiative transfer in a homogeneous cloud layer as a function of its scattering optical thickness, when using the layer average intensity approximation. This increase in computation time is mainly due to the splitting of thick model layers into thin sublayers, needed to make the approximation of Eq. (15) valid, which increases the size of $\mathbf{M}$. Also, the iteration to solve matrix equation $\mathbf{M\Phi} = \mathbf{C}$ converges more slowly with increasing scattering optical thickness, due to the higher order of scattering in cloudy model layers.

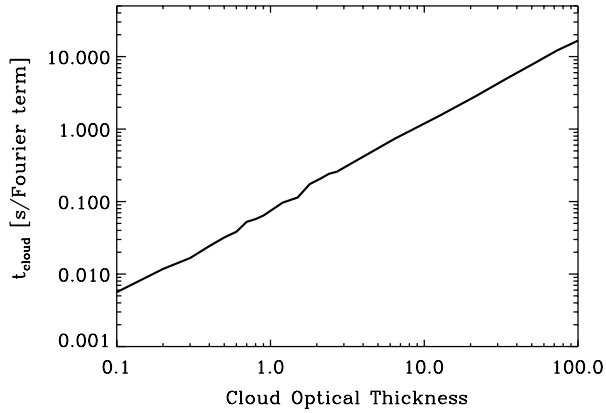

Fig. 1. Mean calculation time t_{cloud} per Fourier term of the intensity field in a nonabsorbing cloud layer as a function of the scattering optical thickness of the cloud layer, when using the layer average intensity approximation. The scattering properties of the cloud layer are described by Mie theory. Cloud particles with a two-parameter gamma distribution, an effective radius of 6 μm, an effective variance of 0.5 μm, and a refractive index of 1.335 are taken. The scattering properties are calculated at 550 nm. The scattering optical thickness threshold for the layer splitting Δ_{scat} is taken to be 0.01, yielding an accuracy of 10^{-2}% (Ref. 32). In these calculations, a nadir viewing geometry is taken with a solar zenith angle of 40°. Furthermore circular polarization is neglected and 64 Gaussian streams are used. The calculations are performed on a Pentium 4 2.8 GHz computer.

Because the layer average intensity approximation is commonly used in combination with the Gauss–Seidel technique to solve matrix Eq. (12), we refer to this combination simply as the Gauss–Seidel technique in the remainder of this paper.

C. Doubling Method for Optically Thick Layers

As discussed in Subsection 2.B, the Gauss–Seidel technique is not efficient to solve the radiative transfer in optically thick layers. Alternatively, when the reflection and transmission properties of these layers are known, $\boldsymbol{\alpha}_k^m$ and $\boldsymbol{\beta}_k^m$ can be defined for these layers by

$$\boldsymbol{\alpha}_k^m(\mu_j,\ \mu_i) = \boldsymbol{\alpha}_k^m(\mu_{-j},\ \mu_{-i}) = \boldsymbol{\beta}_k^m(\mu_{-j},\ \mu_i)$$

$$= \boldsymbol{\beta}_k^m(\mu_j,\ \mu_{-i}) = 0, \tag{19}$$

$$\boldsymbol{\alpha}_k^m(\mu_{-j},\ \mu_i) = 2\mu_j \mathbf{R}_k^m(\mu_j,\ \mu_i),$$

$$\boldsymbol{\alpha}_k^m(\mu_j,\ \mu_{-i}) = 2\mu_j \mathbf{R}_k^{*m}(\mu_j,\ \mu_i),$$

$$\boldsymbol{\beta}_k^m(\mu_{-j},\ \mu_{-i}) = 2\mu_j \mathbf{T}_k^m(\mu_j,\ \mu_i) + \delta_{ij} \times \exp(-\Delta\tau_k/\mu_i \mathbf{E}),$$

$$\boldsymbol{\beta}_k^m(\mu_j,\ \mu_i) = 2\mu_j \mathbf{T}_k^{*m}(\mu_j,\ \mu_i) + \delta_{ij} \times \exp(-\Delta\tau_k/\mu_i \mathbf{E}), \tag{20}$$

and $\boldsymbol{\gamma}_k^m$ can be defined by

$$\boldsymbol{\gamma}_k^m(\mu_i) = \frac{\mu_0}{\pi}\, \mathbf{R}_k^m(\mu_0,\ \mu_i),$$

$$\boldsymbol{\gamma}_k^m(\mu_{-i}) = \frac{\mu_0}{\pi}\, \mathbf{T}_k^m(\mu_0,\ \mu_i), \tag{21}$$

with $i, j = 1, \ldots, N$. Here $\mathbf{R}_k^m$ and $\mathbf{T}_k^m$ are the mth Fourier terms of the reflection and transmission matrices, respectively, for light incident on the upper boundary of the layer. The Fourier terms of the reflection and transmission matrices for light incident on the lower boundary of the layer are denoted by $\mathbf{R}_k^{*m}$ and $\mathbf{T}_k^{*m}$.

An efficient method for calculating the reflection and transmission matrices of homogeneous cloud layers is the doubling method.[23,36] To briefly explain the doubling method, we consider a model atmospheric layer with the scattering optical thickness $\Delta\tau$, of which the reflection and transmission properties are known. This layer is then placed on another identical layer. The reflection and transmission properties of the combined layer with optical thickness $2\Delta\tau$ can now be calculated using the doubling equations given by de Haan *et al.*[23] Repeatedly, the resulting layer can be placed on another identical layer, and the reflection and transmission properties of this combined layer can be calculated. Thus repeating this procedure N times, the reflection and transmission properties of a homogeneous layer with optical thickness $2^N\Delta\tau$ are obtained. Therefore the doubling method is an efficient method to calculate the reflection and transmission properties of optically thick homogeneous layers. The doubling method is started with a layer having a scattering optical thickness small enough so that the two orders of scattering approximation are valid. The reflection and transmission properties of this initial layer can be calculated analytically as described by Hovenier.[36] A detailed discussion of the doubling method is given by de Haan *et al.*[23]

3. Combined Doubling and Gauss–Seidel Model: Validation and Numerical Performance

Based on the theory discussed in Section 2, we introduce the CODAGS model to efficiently perform monochromatic radiative transfer calculations in inhomogeneous atmospheres, which contain a limited number of homogeneous cloud layers. In this model, the radiative transfer problem is solved using the matrix equation [Eq. (12)], for which the coefficients are calculated as described in Subsection 2.C for a cloud layer, and as described in Subsection 2.B for the rest of the atmosphere. We will discuss the efficiency and accuracy of the CODAGS model.

Table 1. Used Settings of the CODAGS

TOA Accuracy ϵ [%]	Settings	
	Δ_{scat}	ϵ_{cloud}
10^{-1}	10^{-1}	10^{-4}
10^{-2}	10^{-2}	10^{-5}
10^{-4}	10^{-3}	10^{-7}

The accuracy of the CODAGS model is, on the one hand, determined by the optical thickness thresholds (Δ_{scat}) used to split the model layers in the Gauss–Seidel method [see Eq. (15)]. On the other hand, the CODAGS accuracy depends on the optical thickness of the initial layer used in the doubling method for the calculation of the reflection and transmission properties of the cloud layer. For the doubling calculations, the absolute accuracy ϵ_{cloud} can be specified beforehand as described by de Haan *et al.*[23] In principle, both the Gauss–Seidel and the doubling methods can obtain an arbitrary accuracy. However, there is a strong trade-off between accuracy and computational effort for both methods and thus for the CODAGS model. Here, especially, Δ_{scat} in the Gauss–Seidel method plays a crucial role. We investigate the computational speed of CODAGS for several accuracies. The settings of Δ_{scat} and ϵ_{cloud} used are given in Table 1. As a reference, we use doubling–adding calculations with an accuracy of approximately 10^{-8}%.

For all calculations, a nadir viewing geometry with a solar zenith angle of 40° is taken. Furthermore, a 30-layered U.S. standard[37] Rayleigh scattering nonabsorbing model atmosphere is used containing one homogeneous cloud layer with properties as described in the caption of Fig. 1. The cloud layer has an optical thickness of 20 and a geometrical thickness of 1 km. The cloud top height is chosen at 3 km. To account for the highly peaked scattering phase function in the cloud layer, we use the so-called MS method of Nakajima and Tanaka.[38] In this method, the radiative transfer of multiple-scattered light is calculated using the δ-M approximation, whereas the contribution of single-scattered light is calculated analytically. Furthermore, we use 64 Gaussian-quadrature streams, i.e., $N = 32$ in Eq. (2). Circular polarization is neglected, since its contribution is relatively small for the considered atmospheres.[16] All calculations are performed on a Pentium 4 2.8 GHz computer.

For radiative transfer calculations in a model atmosphere containing one homogeneous cloud layer,

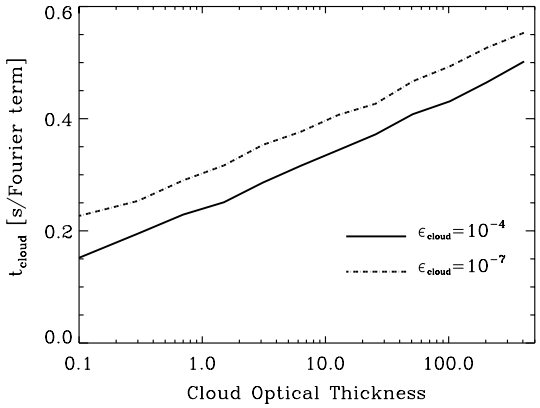

Fig. 2. Mean calculation time t_{cloud} per Fourier term of the reflection and transmission matrices **R** and **T** as a function of the cloud optical thickness. The solid and dashed curves correspond to absolute accuracies ϵ_{cloud} of 10^{-4} and 10^{-7}, respectively.

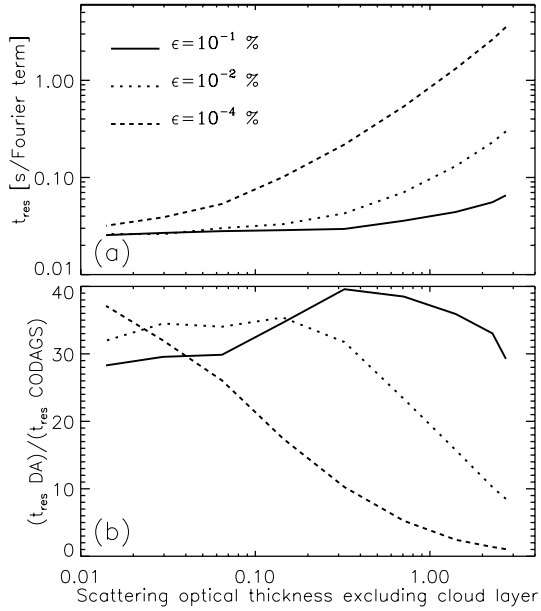

Fig. 3. Mean residual computation time per Fourier term as a function of the total scattering optical thickness using CODAGS. (a) Absolute calculation time t_{res}. (b) t_{res} relative to the corresponding doubling–adding (DA) calculations. Solid, dotted, and dashed curves are for accuracies of 10^{-1}, 10^{-2}, and 10^{-4}%, respectively.

the total calculation time t_{tot} can be written as $t_{tot} = t_{cloud} + t_{res}$, where t_{cloud} is the time needed for the calculation of the reflection and transmission matrices of the cloud, and t_{res} is the residual calculation time needed for the radiative transfer calculation in the noncloudy part of the atmosphere. In Fig. 2, t_{cloud} per Fourier term is shown as a function of cloud optical thickness for two absolute accuracies. A comparison of Fig. 2 with Fig. 1 shows that the doubling method is the most efficient for clouds with an optical thickness above approximately 2, whereas the Gauss–Seidel method is the most efficient for a lower cloud optical thickness.

To study the numerical effort of CODAGS, we compare the computation times t_{tot} and t_{res} of CODAGS with that of the doubling–adding calculations using the model of de Haan *et al.*[23] for similar accuracies. We note that the invariant imbedding method,[39] which is also based on the adding equations, might be more efficient than the doubling–adding technique in some cases. Because both the doubling–adding model and CODAGS use the doubling method for the calculation of the cloud reflection and transmission properties, t_{cloud} is the same in both models. For CODAGS, Fig. 3 shows t_{res} as a function of scattering optical thickness in the noncloudy part of the model atmosphere. CODAGS is about 10–30 times faster than the doubling–adding calculations for an accuracy of 10^{-2}%. For higher accuracies and large scattering optical thicknesses, the efficiency of CODAGS is decreased strongly. However, these higher accuracies are generally not needed for the interpretation of satellite measurements.

The relative calculation times mentioned above hold for one incoming solar angle. This is generally the calculation needed in retrieval algorithms. If simultaneous calculations are to be made for several incoming angles, e.g., for the calculation of lookup tables, the efficiency of CODAGS relative to that of the doubling–adding method decreases because the doubling–adding method provides reflection and transmission properties of the atmosphere for a large set of solar zenith angles. However, the CODAGS method can be adapted for this purpose by replacing the Gauss–Seidel method for solving the matrix equation [Eq. (12)] by the LU decomposition method.[30,32]

The high efficiency of CODAGS becomes less clear when we consider the total computation time t_{tot}, which also includes the numerical calculation for the cloud layer. Here, t_{tot} is only 3–5 times larger for the doubling–adding calculations than for CODAGS with an accuracy of 10^{-2}%. This is because the total computation time is dominated by the calculations for the cloud layer. Thus to take advantage of the high efficiency of CODAGS for the noncloudy part, t_{cloud} has to be reduced. This will be discussed in Section 5.

The calculation times given in Figs. 3 and 4 represent simulations per Fourier term for Fourier terms with a full coupling between the cloud layer and the noncloudy part of the atmosphere. However, if $\mathbf{Z}^m = 0$ [see Eq. (18)] for layers other than the cloud layer and $\mathbf{Z}^m \neq 0$ for the cloud layer itself, essentially $t_{res} = 0$ and $t_{tot} = t_{cloud}$, both for CODAGS and the doubling–adding code. This situation occurs, for example, for Fourier terms $m > 2$ in a Rayleigh scattering atmosphere containing cloud layers with an off-nadir viewing and off-zenith solar geometry. However, for cloudy atmospheres with an additional aerosol loading, the results shown in Figs. 3 and 4 are representative for all Fourier terms. For a detailed discussion on the required number of Fourier terms we refer to King.[40]

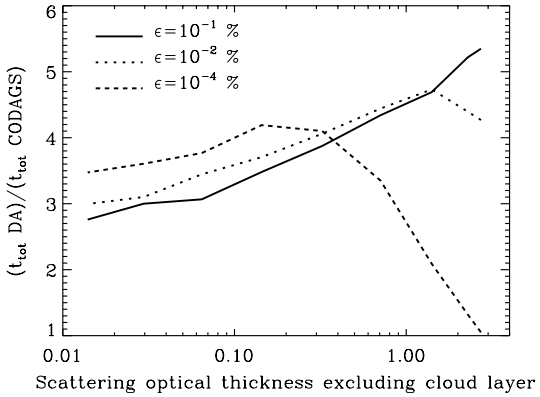

Fig. 4. Mean total computation time t_{tot} per Fourier term as a function of the total scattering optical thickness using CODAGS, relative to the corresponding doubling–adding calculations. The model atmosphere contains one cloud layer with a scattering optical thickness of 20. Solid, dotted, and dashed curves are for accuracies of 10^{-1}, 10^{-2}, and 10^{-4}%, respectively.

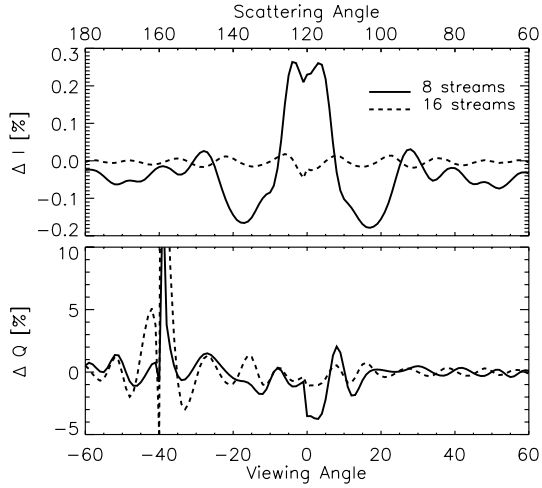

Fig. 5. Errors in I and Q due to the reduction of the Gaussian-quadrature streams in the noncloudy part of the model atmosphere as a function of the viewing angle. The corresponding single scattering angle is indicated at the top axis. A solar zenith angle of 60° and a relative azimuth angle of 0° are used. For the calculation of the cloud properties, 64 Gaussian-quadrature streams are used. The solid and dashed curves show the errors made when 8 or 16 streams are used in the Gauss–Seidel calculations, respectively. A total Rayleigh scattering optical thickness of 0.8 is taken, corresponding to a wavelength of 330 nm.

4. Reduction of Gaussian-Quadrature Streams

In radiative transfer calculations for Rayleigh and/or aerosol scattering atmospheres containing cloud layers, commonly the same number of Gaussian-quadrature streams [see Eq. (2)] is used in all model layers of the atmosphere. The number of streams needed to obtain a required accuracy depends on the shape of the considered scattering phase matrices, in particular on their peakedness.[38] In general, cloud droplets have highly peaked scattering phase matrices in the UV to near-infrared wavelength region.[17] Therefore to describe phase matrices of cloud particles, more streams are needed then to describe Rayleigh or aerosol phase matrices. The separation of the cloudy and noncloudy part of the model atmosphere for the solution of the radiative transfer equation, as done in CODAGS, suggests using a lower number of streams for the noncloudy part. This will reduce the computation time t_{res} significantly with only a minor loss in accuracy. To obtain the reflection and transmission matrices of the cloud layer for the streams used in the noncloudy part of the model atmosphere, an interpolation is used. Following a suggestion of Knibbe *et al.*,[41] we employ a bicubic spline algorithm[30] for this interpolation.

To illustrate the errors due to this approach, simulations of backscattered sunlight are performed for a nonabsorbing Rayleigh scattering model atmosphere containing one cloud layer. Using 64 streams for the cloud layer, Fig. 5 shows the resulting error as a function of the viewing angle, when using 8 or 16 streams in the noncloudy part of the model atmosphere, instead of 64. Errors in I are below 0.3% and 0.05% using 8 and 16 streams, respectively. Errors in Q are generally below 4% and 1.2% using 8 and 16 streams, respectively, except for the region around a scattering angle of 160° where Q is nearly 0. The errors in Fig. 5 mainly result from the decrease in coupling between the cloud layer and the surrounding layers. Results shown in Fig. 5 are for a total Rayleigh scattering optical thickness of 0.8. Generally, similar or lower errors are obtained for other values of the total Rayleigh scattering optical thickness. Reducing the number of streams from 64 to 8 and 16, decreases t_{res} by a factor of approximately 80 and 20, respectively.

5. Interpolation of the Cloud Reflection and Transmission Matrices

In Section 3, we showed that the CODAGS model is highly efficient for radiative transfer calculations in the noncloudy part of an inhomogeneous model atmosphere. However, the radiative transfer calculations in the cloudy part dominate the total calculation time, which is still too large for many practical applications, such as the retrieval of cloud properties or trace gases in cloudy atmospheres, for which many spectral calculations in a given absorption band have to be performed. Therefore an interpolation technique is proposed to significantly reduce the number of cloud calculations in a given spectral absorption band.

For the radiative transfer in absorption bands, various approximation techniques have been proposed previously to reduce the computing time (e.g., Refs. 18 and 42). The underlying basic method of most of these techniques is the so-called correlated k-distribution method. However, due to the uncorrelated nature of overlapped absorption lines, these techniques can yield large errors in atmospheres containing clouds, especially in strong absorption bands such as the oxygen A band.[43] The recently published double-k approach[43] significantly reduces these errors and obtains high accuracies (<0.5%) in the oxy-

gen A band for atmospheres containing one cloud layer. The concept of CODAGS allows us to easily overcome any problem due to the uncorrelated nature of overlapping absorption bands. Utilizing the high level of performance of the CODAGS model in the noncloudy part, we calculate the radiative transfer in this part of the atmosphere line by line. To reduce the numerical effort needed to calculate the transmission and reflection matrices of a homogeneous cloud layer, we make use of the fact that these matrices depend smoothly on the total (absorption) optical depth, a feature that is also used by k-distribution methods. Consequently, an interpolation scheme using calculations of the reflection and transmission properties of the cloud layer at selected optical depths allows one to efficiently incorporate a cloud layer in the CODAGS model. Since the cloud layer is assumed to be optically homogeneous, a correlation problem does not exist for this layer, and therefore the approach converges to the accurate solution for an increasing number of interpolation points. Furthermore, unlike the k-distribution methods, our approach allows us to specify an approximate accuracy beforehand, and it can be used in any wavelength range including a variation in scattering properties.

By means of the oxygen A absorption band around 760 nm, which is often used for the retrieval of cloud properties,[9,12,14] we will demonstrate how the reflection and transmission matrices of a cloud layer can be interpolated over absorption optical thickness in the cloud layer. This interpolation is applied separately to each Fourier term. For the first Fourier term, Figs. 6(a) and 6(b) show element R_{11} of the cloud reflection matrix as a function of wavelength and the absorption optical thickness in the cloud, respectively. From Fig. 6 it follows that the cloud reflection and transmission matrices vary smoothly as a function of absorption optical depth in the cloud when evaluated at a fixed scattering optical depth. Thus the elements of the cloud reflection and transmission matrices can be obtained by interpolation, from radiative transfer calculations at a reduced number N_{abs} of absorption optical depths in the cloud layer. The computational effort of the linear interpolation used is negligible. When the reflection and transmission matrices vary significantly with scattering optical depth as well, a double interpolation has to be performed over both the scattering and absorption optical depths. When evaluating the reflection and transmission matrices at N_{scat} values of the scattering optical depths in the cloud layer, a total of $N_{\mathrm{abs}} \times N_{\mathrm{scat}}$ radiative transfer calculations have to be performed. Since the reflection and transmission matrices vary approximately linearly with scattering optical depth in the cloud layer, generally errors below $10^{-2}\%$ are obtained when taking $N_{\mathrm{scat}} = 2$. Moreover, when the range of scattering optical depths in the considered band is smaller than 0.005, errors below $10^{-2}\%$ are obtained when the scattering optical thickness is fixed at its average value, denoted as $N_{\mathrm{scat}} = 1$.

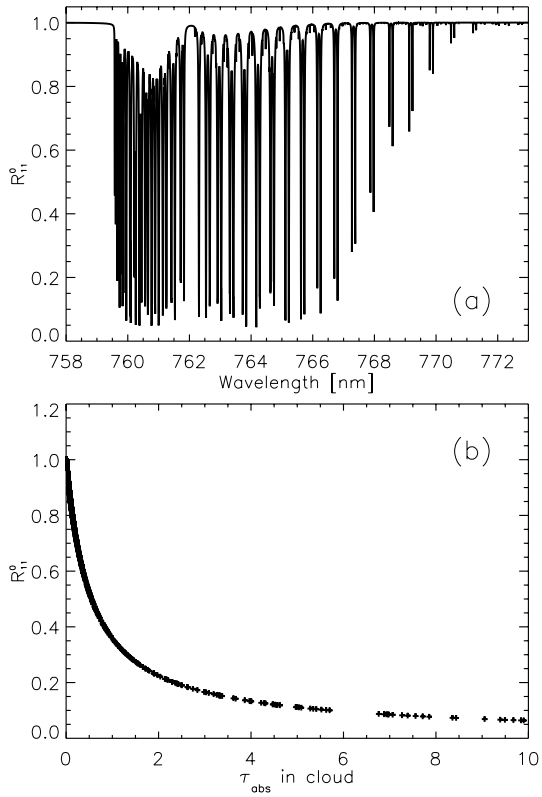

Fig. 6. (a) Normalized element R^0_{11} of the cloud reflection matrix as a function of the wavelength and (b) as a function of absorption optical depth in the cloud layer for the fixed scattering optical depth. The calculations are performed on a 0.005 nm spectral grid (3000 wavelengths in total) with a solar zenith angle of 40°, a viewing angle of 20°, and a relative azimuth angle of 0°. Absorption cross sections are taken from the HITRAN2004 database (Ref. 44). The atmospheric setup as presented in Section 3 is used throughout this section, unless specified otherwise.

For a given absorption band, the error due to this interpolation depends on the number of interpolation points and their distribution over the optical depths. A scheme to determine the distribution of interpolation points over the absorption optical depths to obtain a required accuracy in $\mathbf{I}$ is described in Appendix B. In principle, accuracies can be specified for each Stokes parameter, but it mostly suffices to only specify an accuracy on the Stokes parameter I. In the interpolation scheme, first a range of absorption optical depths in which the interpolation has to be performed is determined. Then interpolation points are added until the error on $\mathbf{I}$ due to this interpolation is estimated to be below the required accuracy for all absorption optical depths. The distribution of interpolation points is calculated for each Fourier term separately. Generally, for increasing Fourier term m, the relative contribution of $\mathbf{I}^m$ to the total intensity vector decreases. Therefore the required number of interpolation points decreases with the Fourier index.

Figure 7 shows the difference between calculations in the oxygen A band at 3000 wavelengths performed with a line-by-line model and one using the interpolation scheme. The number of interpolation points

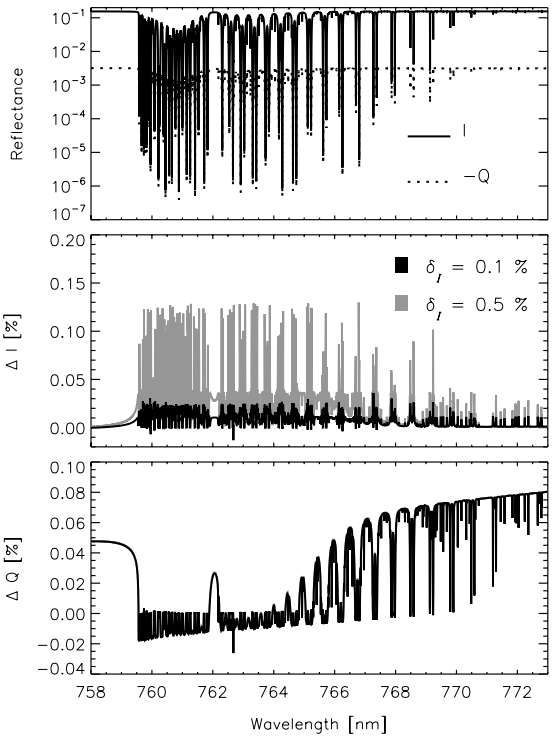

Fig. 7. Modeled Stokes parameters I and Q in the oxygen A band at 3000 wavelengths (top panel) and the differences ΔI (middle panel) and ΔQ (bottom panel) between calculations performed with a line-by-line model and calculations performed using the interpolation scheme with $\delta_I = 0.1\%$ and $\delta_I = 0.5\%$. The same atmospheric setup is used as in Fig. 6. The Fourier series is truncated at a maximum of 28 terms.

corresponds to a required accuracy in the Stokes parameter I of $\delta_I = 0.1\%$ and $\delta_I = 0.5\%$. For several cloud top heights, Fig. 8 shows the required number of interpolation points, N_{abs}, for the first Fourier term as a function of accuracy. With increasing cloud height, the total absorption optical thickness above the cloud decreases, increasing the relative contribution of light reflected by the cloud to the top of the atmosphere intensity. As a result, the required number of interpolation points increases with cloud height. For accuracies of 0.02% to 1%, 140 to 18 interpolation points are needed for the first Fourier term. For the second and third Fourier terms, three to nine interpolation points are required to obtain these accuracies. For higher terms, three interpolation points are mostly sufficient. The required number of interpolation points is found to be rather independent of geometry. Furthermore, the range of the scattering optical thickness in the cloud layer is 0.0002, which means that using $N_{\text{scat}} = 1$ is sufficient, as discussed above. As a result, in the example shown in Fig. 7 with $\delta_I = 0.1\%$ and $\delta_I = 0.5\%$, the total number of calculations for the cloud matrices is reduced by a factor of 576 and 761, respectively.

To illustrate the application of our interpolation scheme for spectral ranges where the scattering optical thickness also varies significantly with the wavelength, it is applied to calculations in the

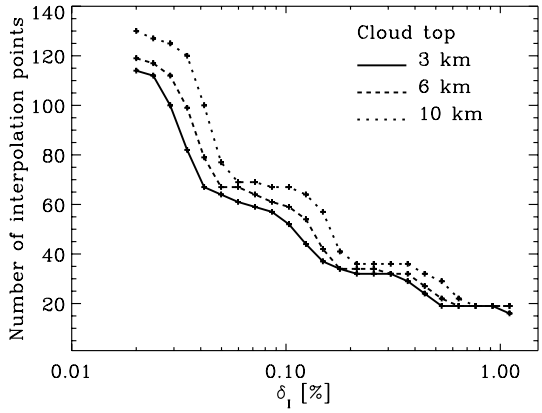

Fig. 8. Required number of interpolation points for the first Fourier term as a function of the relative accuracy of I at the top of the atmosphere in the oxygen A band. Solid, dashed, and dotted curves correspond to cloud top heights of 3, 6, and 10 km, respectively. The number of interpolation points are calculated using the scheme described in Appendix B.

Hartley–Huggins ozone absorption band from 295 to 335 nm at 400 wavelengths. This band is often used for the retrieval of ozone profiles and total ozone columns.[10,45] In this band, the range of scattering optical thickness in the cloud layer is 0.05 due to Rayleigh scattering. Therefore we set $N_{\text{scat}} = 2$. The interpolation points required for the interpolation over absorption optical depths are determined by the scheme presented in Appendix B. The resulting errors for $\delta_I = 0.5\%$ are shown in Fig. 9. The obtained accuracy is well below 0.5%. Since the range in absorption optical depth in the cloud layer is much smaller in the ozone band as compared to that in the oxygen A band, the reflection and transmission matrices are more linear and only three interpolation points for each Fourier term are required for the interpolation over absorption optical depths. As a result, in this example the total number of calculations for the cloud matrices is reduced by a factor of 55.

6. Simulation of Scanning Imaging Absorption Spectrometer for Atmospheric Cartography Measurements

To demonstrate the practical use of the CODAGS radiative transfer model, including the reduction of streams and the interpolation technique discussed in Sections 4 and 5, respectively, it is applied to the simulation of measurements from the spaceborne spectrometer SCIAMACHY[2] in the Hartley–Huggins ozone band and oxygen A band, as shown in Figs. 7 and 9, respectively. Since the SCIAMACHY is a polarization-sensitive instrument, the intensity I_{pol} measured at a certain wavelength λ is determined not only by the intensity of the light that enters the instrument but also by its state of polarization,[47,48] viz.

$$I_{\text{pol}}(\lambda) = I_{\text{TOA}}(\lambda) + m_{12}(\lambda) Q_{\text{TOA}}(\lambda), \tag{22}$$

where m_{12} is an element of the instrument's Müller matrix normalized to its element (1, 1) and assumed to be 0.4 at the considered wavelengths. The rela-

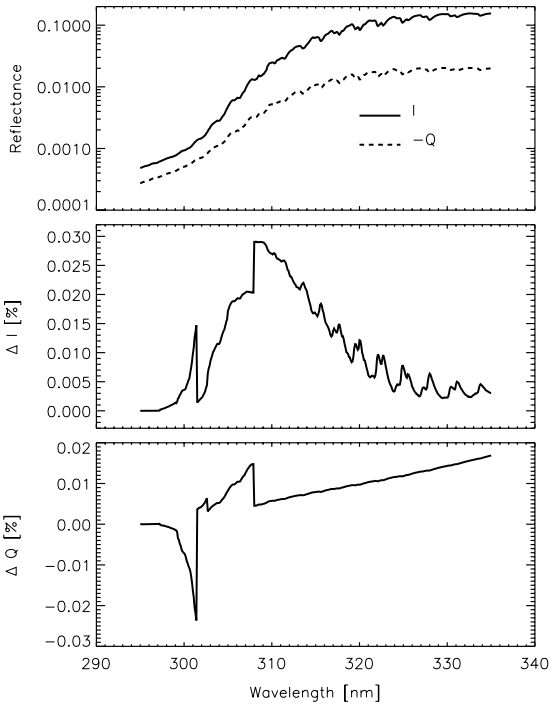

Fig. 9. Same as Fig. 7 but for the Hartley–Huggins ozone absorption band. $\delta_I = 0.5\%$ and $N_{\mathrm{scat}} = 2$. The calculations are performed on a 0.1 nm wavelength grid at 400 wavelengths in total. The ozone absorption cross sections are taken from Bass and Paur.[46] The Fourier series is truncated at a maximum of 16 terms.

tively small sensitivity of the SCIAMACHY to U is neglected. Furthermore, I_{TOA} and Q_{TOA} are the first two elements of the intensity vector at the top of the atmosphere convolved with the instruments response function, which is approximated by a Gaussian with a FWHM of 0.4 nm. The SCIAMACHY has a typical noise level of 0.1%–0.5% in the UV and visible wavelength ranges. Therefore errors in I below 0.1% need to be obtained at the SCIAMACHY's resolution. The required accuracy in Q depends on the degree of polarization. In atmospheres containing clouds, the degree of polarization is typically <30% at a scattering angle around 140° (the so-called rainbow geometry) and <10% at other geometries.[16,17] Because m_{12} is 0.4, errors in Q at the SCIAMACHY's resolution need to be below approximately 1% in the rainbow geometry and 2.5% in other geometries. We found that these requirements are met in the oxygen A band when δ_I is set to 0.5%, $N_{\mathrm{scat}} = 1$, and eight streams are used in the noncloudy part of the atmosphere. In the ozone absorption band, the requirements are met when 16 streams are used in the noncloudy part of the atmosphere, δ_I is set to 0.5%, and $N_{\mathrm{scat}} = 2$. Figures 10 and 11 show the resulting errors in I and Q in the oxygen A band and the ozone band, respectively. In both bands, the error due to the interpolation of the cloud matrices is dominant in I, whereas the error in Q is dominated by the reduction in streams, as follows from comparison of Fig. 10 with Fig. 7 and Fig. 11 with Fig. 9.

Using CODAGS with these settings, the calculations

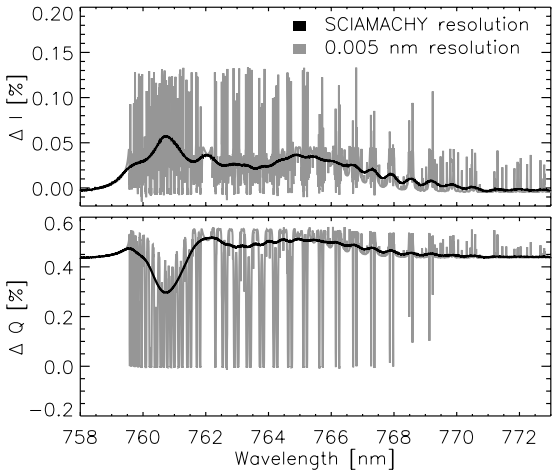

Fig. 10. Accuracy of CODAGS in combination with the proposed interpolation scheme and the reduction of streams for calculations in the oxygen A band at 3000 wavelengths on a 0.005 nm wavelength grid (gray) and at the SCIAMACHY resolution (black). δ_I is set to 0.5%, $N_{\mathrm{scat}} = 1$, and eight streams are used in the noncloudy part of the atmosphere. The same atmospheric setup is used as in Fig. 6. The Fourier series is truncated at a maximum of 28 terms.

in the oxygen A and ozone bands are performed in 60 and 44 s, respectively, on a Pentium 4 2.8 GHz PC. The calculation times are reduced for geometries for which fewer Fourier terms are required.

For retrieval purposes, not only are the outgoing Stokes parameters at the top of the atmosphere needed but also their derivatives with respect to atmospheric properties. Since both the Gauss–Seidel and the doubling models calculate the internal radiation field with no or little extra computational effort,[24,49] these derivatives can be efficiently calculated according to the method described by Hasekamp and Landgraf.[50] Thus CODAGS can be practically used for (off-line) retrieval algorithms.

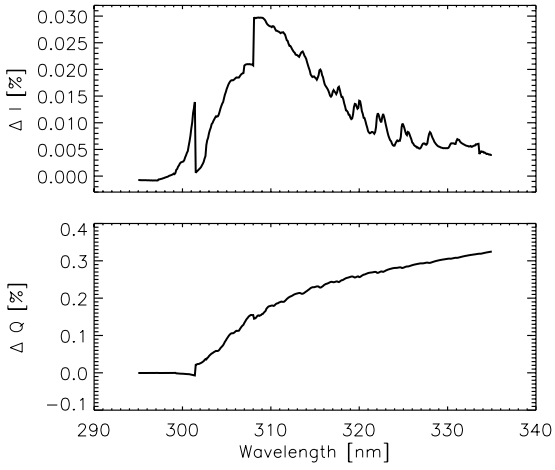

Fig. 11. Same as Fig. 10 but for the Hartley–Huggins ozone band at 400 wavelengths. Sixteen streams are used in the noncloudy part of the atmosphere, $N_{\mathrm{scat}} = 2$, and δ_I is set to 0.5%. The Fourier series is truncated at a maximum of 16 terms.

7. Conclusions

In this paper, we have presented a model to efficiently calculate the radiative transfer of polarized light in atmospheres that contain a limited number of homogeneous cloud layers. This model is based on the concept that the radiative transfer problem in such atmospheres can be written in a matrix equation, which can be efficiently solved using the Gauss–Seidel iteration technique. The elements of this matrix equation are obtained using the commonly used layer average intensity approximation. However, using this approximation is inefficient for optically thick layers. Therefore the elements of the matrix formalism for the optically thick cloud layers are obtained using its reflection and transmission properties calculated with the doubling method. Thus in this combined doubling and Gauss–Seidel (CODAGS) model, for both the optically thin and the optically thick parts of the atmosphere, the most efficient solution techniques are used. Furthermore, it was shown how the number of Gaussian-quadrature streams in the optically thin atmospheric layers can be reduced with respect to those used in the cloud layer, significantly reducing the calculation time. Although an arbitrary number of homogeneous cloud layers can be incorporated in CODAGS, in this paper we restricted the application of CODAGS to atmospheres containing one homogeneous cloud layer because this application is most important for retrieval purposes.

To optimize CODAGS for absorption bands, a method was proposed to reduce the computational effort for high spectral resolution radiative transfer calculations. Since the calculation time for monochromatic calculations in CODAGS is dominated by the calculation of the reflection and transmission matrices of the cloud layer, the number of calculations for these matrices was reduced by interpolating them over the absorption and scattering optical thicknesses within the cloud layer. In the scheme to interpolate over absorption optical thickness, the interpolation points needed to obtain a required accuracy in the top of the atmosphere intensity vector are determined for each Fourier term separately. The number of interpolation points needed to obtain a certain accuracy depends on the strength of the absorption band considered. For example, in the oxygen A band (758–773 nm), the total number of calculations for the cloud reflection and transmission matrices can be reduced by a factor of 576 at an accuracy in I of 0.1%. For calculations in the Hartley–Huggins ozone band (295–335 nm), where the cloud reflection and transmission matrices were also interpolated over the scattering optical thickness in the cloud layer, the total number of calculations for the cloud reflection and transmission matrices can be reduced by a factor of 55 at an accuracy in I below 0.03%.

CODAGS in combination with the proposed interpolation technique is well suited to efficiently simulate high or medium spectral resolution satellite measurements with an accuracy that is more than sufficient for the retrieval of atmospheric parameters. For example, it was shown that accurate simulations of the measurements of the SCIAMACHY instrument in the oxygen A band and the Hartley–Huggins ozone band for an atmosphere containing one homogeneous cloud layer are obtained of the order of 15–60 and 12–45 s, respectively, on a Pentium 4 2.8 GHz PC.

Appendix A: Fourier Expansion for Azimuthal Dependence

To handle the integration of the equations needed in our radiative transfer model over azimuth angles, the Fourier expansion proposed by Hovenier and van der Mee[29] and de Haan *et al.*[23] is used. For the intensity vector at optical depth τ, zenith angle μ, and azimuth angle φ (measured clockwise when looking downward) this expansion is given by

$$\mathbf{I}(\tau,\ \mu,\ \varphi) = \sum_{m=0}^{\infty} (2-\delta_{m0})\big[\mathbf{B}^{+m}(\varphi_o-\varphi)\mathbf{I}^{+m}(\tau,\ \mu) + \mathbf{B}^{-m}(\varphi_o-\varphi)\mathbf{I}^{-m}(\tau,\ \mu)\big], \tag{A1}$$

where φ_o is the azimuth angle of the incoming radiation, δ_{m0} is the Kronecker delta, and

$$\mathbf{B}^{+m}(\varphi) = \mathrm{diag}[\cos m\varphi,\ \cos m\varphi,\ \sin m\varphi,\ \sin m\varphi], \tag{A2}$$

$$\mathbf{B}^{-m}(\varphi) = \mathrm{diag}[-\sin m\varphi,\ -\sin m\varphi,\ \cos m\varphi,\ \cos m\varphi]. \tag{A3}$$

Furthermore the vectors $\mathbf{I}^{+m}$ and $\mathbf{I}^{-m}$ are given by

$$\mathbf{I}^{+m}(\tau,\ \mu) = \frac{1}{2\pi}\int_0^{2\pi} \mathrm{d}\varphi \mathbf{B}^{+m}(\varphi_o-\varphi)\mathbf{I}(\tau,\ \mu,\ \phi),$$

$$\mathbf{I}^{-m}(\tau,\ \mu) = \frac{1}{2\pi}\int_0^{2\pi} \mathrm{d}\varphi \mathbf{B}^{-m}(\varphi_o-\varphi)\mathbf{I}(\tau,\ \mu,\ \phi). \tag{A4}$$

For matrices, this expansion is given by

$$\mathbf{L}(\tau,\ \tilde{\mu},\ \tilde{\phi};\ \mu,\ \phi) = \frac{1}{2}\sum_{m=0}^{\infty}(2-\delta_{m0})\big[\mathbf{B}^{+m}(\tilde{\varphi}-\varphi) \times \mathbf{L}^{m}(\tau,\ \tilde{\mu},\ \mu)(\mathbf{E}+\mathbf{\Delta}) + \mathbf{B}^{-m}(\tilde{\varphi}-\varphi)\mathbf{L}^{m}(\tau,\ \tilde{\mu},\ \mu) \times (\mathbf{E}-\mathbf{\Delta})\big], \tag{A5}$$

where $\mathbf{E}$ is the 4×4 unity matrix and

$$\mathbf{\Delta} = \mathrm{diag}[1,\ 1,\ -1,\ -1]. \tag{A6}$$

$\mathbf{L}$ stands for the matrices used in our model, i.e., the reflection and transmission matrices of a cloud layer,

the reflection matrices of the surface, and the scattering phase matrices.

For the radiative transfer problem with the solar source $\mathbf{F}_0$, defined in Section 2, the Fourier series of Eq. (A1) only contains terms of $\mathbf{I}^{+m}$. Therefore in this paper we omit the positive sign for m.

Appendix B: Scheme to Determine the Distribution of Interpolation Points over the Absorption Optical Depths in the Cloud Layer

For the interpolation of the cloud transmission and reflection matrices over the absorption optical depth in the cloud layer (Section 5), a scheme is presented to determine the distribution of interpolation points to obtain a relative accuracy better than a specified value δ_i in the ith Stokes parameter I_i of the intensity vector $\mathbf{I}$ at the top of the atmosphere. In each step of this scheme, an interpolation point is added, and the relative error in I_i due to the interpolation of the cloud reflection matrix is estimated. When this error can be assumed below δ_i for every absorption optical depth in the cloud layer, the procedure is stopped. For every Fourier term, a new set of interpolation points is determined.

To obtain an accuracy better than δ_i, for each Fourier term M, we require that (see Appendix A)

$$\left|\frac{\left[\sum_{m=0}^{M}(2-\delta_{m0})\mathbf{B}^m(\varphi_o-\varphi)\Delta\mathbf{I}^m(\tau_a)\right]_i}{I_i}\right| < \delta_i, \quad \text{(B1)}$$

where $\Delta\mathbf{I}^m$ is the absolute error in $\mathbf{I}^m$ due to an error in the cloud reflection and transmission matrices with an absorption optical depth τ_a. Neglecting the transmission through the cloud and the multiple scattering above the cloud, I_i in Eq. (B1) is approximated by

$$I_i \approx \left[I_{SS\uparrow} + \sum_{m=0}^{M}(2-\delta_{m0})\mathbf{B}^m(\varphi_o-\varphi)\mathbf{R}_c^m(\tau_a;\ \mu_0,\ \mu)\frac{\mu_0}{\pi} \times \mathbf{F}_0 \exp(-\alpha[\tau_c+\tau_s])\right]_i, \quad \text{(B2)}$$

where $\mathbf{R}_c^m$ is the mth Fourier term of the cloud reflection matrix and $I_{SS\uparrow}$ is the single-scattering solution for the atmosphere above the cloud layer, which can be calculated analytically. Furthermore, τ_c and τ_s are the absorption and scattering optical thicknesses above the cloud layer, respectively, and α is the air mass factor given by $(1/\mu_0 + 1/\mu)$. Again, by neglecting the transmission through the cloud and the multiple scattering above the cloud, $\Delta\mathbf{I}^m$ in Eq. (B1) is approximated by

$$\Delta\mathbf{I}^m(\tau_a) \approx \Delta\mathbf{R}_c^m(\tau_a;\ \mu_0,\ \mu)\frac{\mu_0}{\pi}\mathbf{F}_0\ \exp(-\boldsymbol{\alpha}[\tau_c+\tau_s]), \quad \text{(B3)}$$

where $\Delta\mathbf{R}_c^m(\tau_a;\ \mu_0,\ \mu)$ is the error in the mth Fourier term of the cloud reflection matrix, estimated as explained below. Furthermore, τ_c can be approximated from τ_a using a linear relation, as illustrated in Fig. 12 for the oxygen A band.

The interpolation points are distributed between the minimum absorption optical depth present in the cloud layer $\tau_{\min}$ and a threshold absorption optical depth τ_{thresh}, above which errors in the cloud reflection matrix of 100% or larger can be assumed to result in errors in I_i below δ_i. We first calculate $\mathbf{R}_c^m(\tau_{\min})$. Next, τ_{thresh} is estimated by requiring

$$\frac{\mathbf{R}_c^0(\tau_{\text{thresh}})\exp(-\alpha[\tau_c+\tau_s])}{I_i} = \delta_i. \quad \text{(B4)}$$

In Eq. (B4), $\mathbf{R}_c^0(\tau_{\text{thresh}})$ is not known. Therefore $\mathbf{R}_c^0(\tau_{\min})$ is used instead, which is a conservatively large value because $\mathbf{R}_c^0(\tau_{\min}) > \mathbf{R}_c^0(\tau_{\text{thresh}})$. Furthermore, I_i is approximated by the ith Stokes parameter of $\mathbf{I}_{SS\uparrow}$ ($\tau_c = 0$). We now can obtain τ_c by inverting Eq. (B4) and subsequently determine τ_{thresh} from the linear relation between τ_c and τ_a in Fig. 12. Next, $\mathbf{R}_c^0(\tau_{\text{thresh}})$ is calculated.

The scheme proceeds with two alternating steps 1 and 2. To initialize step 1, the absorption optical depths τ_{a1} and τ_{a2} to be used are taken as $\tau_{\min}$ and τ_{thresh} with the corresponding matrices $\mathbf{R}_c^M(\tau_{\min})$ and $\mathbf{R}_c^M(\tau_{\text{thresh}})$, respectively.

1. The matrix $\mathbf{R}_c^M(\tau_{a3})$ is calculated for $\tau_{a3} = -\ln\{[\exp(-\tau_{a1}) + \exp(-\tau_{a2})]/2\}$. Additionally, $\mathbf{R}_c^M(\tau_{a3})$ is approximated by a linear interpolation between $\mathbf{R}_c^M(\tau_{a1})$ and $\mathbf{R}_c^M(\tau_{a2})$. Then, $\Delta\mathbf{R}_c^M(\tau_{a3})$ is given by the difference between the interpolated and calculated values of $\mathbf{R}_c^M(\tau_{a3})$.
2. When for τ_{a3}, the condition of Eq. (B1) is not fulfilled, the error on the reflection matrix due to interpolation between τ_{a3} and τ_{a2} cannot be assumed to be below δ_i. Then we set $\tau_{a1} = \tau_{a3}$, and the scheme returns to step 1. Otherwise, there are three options:
   (a) If τ_{a1} equals $\tau_{\min}$, the scheme is finished.
   (b) If in the current and previous calculation of step 1, the same value for τ_{a1} was used, the accuracy of the interpolation for all values above τ_{a1} is assumed to be below δ_i. Therefore the scheme returns to step 1 with $\tau_{a2} = \tau_{a1}$ and τ_{a1} taken equal to the closest previously determined interpolation point for which $\tau_{a1} < \tau_{a2}$.
   (c) In all other cases, the interpolation between τ_{a1} and τ_{a3} cannot be assumed below δ_i. Then we set $\tau_{a2} = \tau_{a3}$, and the scheme returns to step 1.

For values of τ_a above τ_{thresh}, the cloud reflection and transmission matrices are interpolated between τ_{thresh} and $\tau_{\max}$, at which the reflection and transmission matrices are assumed to be 0. For $\tau_{\max}$, the value corresponds to the value of τ_c for which $\exp(-\alpha\tau_c) < \epsilon$ is taken. We found that 10^{-12} is a suitable value for ϵ. The cloud reflection and transmission matrices for $\tau_a > \tau_{\max}$ are set to 0.

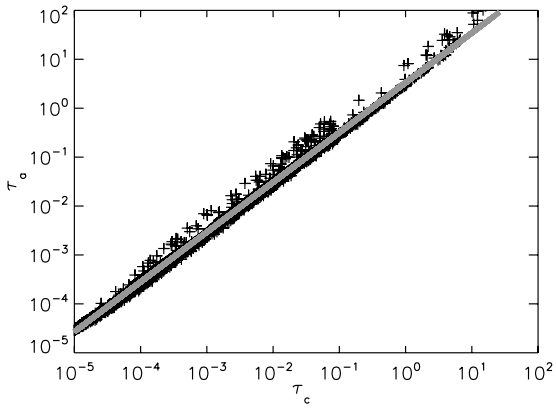

Fig. 12. Absorption optical depth above the cloud layer τ_c as a function of the absorption optical depth in the cloud layer τ_o for the oxygen A band. The least-squares linear fit is shown in gray. A cloud at an altitude of 10 km and a geometrical thickness of 1 km is taken.

It is important to note that some assumptions made in this scheme, i.e., only single scattering above the cloud and illumination of the cloud only by direct sunlight, become less valid at wavelengths for which the Rayleigh scattering cross sections are larger. This will result in an overestimation of the error calculated by Eq. (B1). As a result, the scheme overestimates the required number of interpolation points for short wavelengths, resulting in a higher accuracy than requested.

References

1. J. P. Burrows, M. Weber, M. Buchwitz, V. Rozanov, A. Ladstätter-Weißenmayer, A. Richter, R. de Beek, R. Hoogen, K. Bramstedt, K. Eichmann, M. Eisinger, and D. Perner, "The Global Ozone Monitoring Experiment (GOME): mission concept and first scientific results," J. Atmos. Sci. **56,** 151–175 (1999).
2. H. Bovensmann, J. P. Burrows, M. Buchwitz, J. Frerick, S. Noel, V. V. Rozanov, K. V. Chance, and A. P. H. Goede, "SCIAMACHY: mission objectives and measurement modes," J. Atmos. Sci. **56,** 127–150 (1999).
3. P. F. Levelt, G. H. Oord, E. Hilsenrath, P. K. Bhartia, G. W. Leppelmeier, and A. Malkki, "Science goals of EOS-aura's Ozone Monitoring Instrument (OMI)," EOS Trans. AGU **84**, Fall Meet. Suppl., Abstract A12C-03 (2003).
4. J. M Krijger, M. van Weele, I. Aben, and R. Frey, "The effect of sensor resolution on the number of cloud-free observations from space," Atm. Chem. Phys. Discuss. **6**, 4465–4494 (2006).
5. A. M. Thompson, D. P. McNamara, K. E. Pickering, and R. D. McPeters, "Effect of marine stratocumulus on TOMS ozone," J. Geophys. Res. [Atmos.] **98,** 23051–23057 (1993).
6. R. B. A. Koelemeijer and P. Stammes, "Effects of clouds on ozone column retrieval from GOME UV measurements," J. Geophys. Res. [Atmos.] **104,** 8281–8294 (1999).
7. T. Kurosu, V. V. Rozanov, and J. P. Burrows, "Parameterization schemes for terrestrial water clouds in the radiative transfer model GOMETRAN," J. Geophys. Res. [Atmos.] **102,** 21809–21824 (1997).
8. A. A. Kokhanovsky, "Reflection of light from nonasbsorbing semi-infinite cloudy media: a simple approximation," J. Quant. Spectrosc. Radiat. Transfer **85,** 25–33 (2004).
9. R. B. A. Koelemeijer, P. Stammes, J. W. Hovenier, and J. F. de Haan, "A fast method for retrieval of cloud parameters using oxygen A band measurements from the Global Ozone Monitoring Experiment," J. Geophys. Res. [Atmos.] **106,** 3475–3490 (2001).
10. X. Liu, M. J. Newchurch, R. Loughman, and P. K. Bhartia, "Errors resulting from assuming opaque Lambertian clouds in TOMS ozone retrieval," J. Quant. Spectrosc. Radiat. Transfer **85,** 337–365 (2004).
11. Z. Ahmad, P. K. Bhartia, and N. Krotkov, "Spectral properties of backscattered UV radiation in cloudy atmospheres," J. Geophys. Res. [Atmos.] **109,** D01201, doi:10.1029/2003JD003395 (2004).
12. J. Fischer and H. Grassl, "Detection of cloud-top height from backscattered radiances within the oxygen A band. Part 1: Theoretical study," J. Appl. Meteorol. **30,** 1245–1259 (1991).
13. J. S. Daniel, S. Solomon, H. L. Miller, A. O. Langford, R. W. Portmann, and C. S. Eubank, "Retrieving cloud information from passive measurements of solar radiation absorbed by molecular oxygen and O_2–O_2," J. Geophys. Res. [Atmos.] **108,** D16, 4515, doi:10.1029/2002JD002994 (2003).
14. V. V. Rozanov and A. A. Kokhanovsky, "Semianalytical cloud retrieval algorithm as applied to the cloud top altitude and the cloud geometrical thickness determination from top-of-atmosphere reflectance measurements in the oxygen A band," J. Geophys. Res. [Atmos.] **109,** D05202, doi: 10.1029/2003JD004104 (2004).
15. M. Wang and M. D. King, "Correction of Rayleigh scattering effects in cloud optical thickness retrievals," J. Geophys. Res. [Atmos.] **102,** 25915–25926 (1997).
16. J. E. Hansen, "Multiple scattering of polarized light in planetary atmospheres. Part II. Sunlight reflected by terrestrial water clouds," J. Atmos. Sci. **28,** 1400–1426 (1971).
17. K. Liou, *Radiation and Cloud Processes in the Atmosphere* (Oxford U. Press, 1992).
18. D. M. Stam, J. F. De Haan, J. W. Hovenier, and I. Aben, "Detecting radiances in the O_2 A band using polarization-sensitive satellite instruments with application to the Global Ozone Monitoring Experiment," J. Geophys. Res. **105**(D17), 22379–22392 (2000).
19. A. Kokhanovsky and R. Weichert, "Determination of the droplet effective size and optical depth of cloudy media from polarimetric measurements: theory," Appl. Opt. **41,** 3650–3658 (2002).
20. P. Y. Deschamps, F. M. Breon, M. Leroy, A. Podaire, A. Bricaud, J. C. Buriez, and G. Seze, "The POLDER mission: instrument characteristics and scientific objectives," IEEE Trans. Geosci. Remote Sens. **32,** 598–615 (1994).
21. M. I. Mishchenko, B. Cairns, J. E. Hansen, L. D. Travis, R. Burg, Y. J. Kaufman, J. Vanderlei Martins, and E. P. Shettle, "Monitoring of aerosol forcing of climate from space: analysis of measurement requirements," J. Quant. Spectrosc. Radiat. Transfer **88,** 149–161 (2004).
22. F. Parol, J. C. Buriez, C. Vanbauce, J. Riedi, L. C. Labonnote, M. Doutriaux-Boucher, M. Vesperini, G. Sèze, P. Couvert, M. Viollier, and F. M. Bréon, "Review of capabilities of multi-angle and polarization cloud measurements from POLDER," Adv. Space Res. **33,** 1080–1088 (2004).
23. J. F. de Haan, P. Bosma, and J. W. Hovenier, "The adding method for multiple scattering calculations of polarized light," Astron. Astrophys. **181,** 371–391 (1987).
24. O. P. Hasekamp and J. Landgraf, "A linearized vector radiative transfer model for atmospheric trace gas retrieval," J. Quant. Spectrosc. Radiat. Transfer **75,** 221–238 (2002).
25. F. M. Schulz, K. Stamnes, and F. Weng, "Vdisort: an improved and generalized discrete ordinate method for polarized (vector) radiative transfer," J. Quant. Spectrosc. Radiat. Transfer **61,** 105–122 (1999).
26. A. A. Kokhanovsky, "Reflection and transmission of polarized light by optically thick weakly absorbing random media," J. Opt. Soc. Am. A **18,** 883–887 (2001).

27. A. A. Kokhanovsky and V. V. Rozanov, "The physical parameterization of the top-of-atmosphere reflection function for a cloudy atmosphere-underlying surface system: the oxygen A-band case study," J. Quant. Spectrosc. Radiat. Transfer **85,** 35–55 (2004).
28. S. Chandrasekhar, *Radiative Transfer* (Dover, 1960).
29. J. W. Hovenier and C. V. M. van der Mee, "Fundamental relationships relevant to the transfer of polarized light in a scattering atmosphere," Astron. Astrophys. **128,** 1–16 (1983).
30. W. H. Press, S. A. Teukolsky, W. T. Vetterling, and B. P. Flannery, *Numerical Recipes in FORTRAN. The Art of Scientific Computing,* 2nd ed. (Cambridge U. Press, 1992).
31. B. Herman and S. Browning, "A numerical solution to the equation of radiative transfer," J. Atmos. Sci. **22,** 559–566 (1965).
32. J. Landgraf, O. P. Hasekamp, T. Trautmann, and M. A. Box, "A linearized radiative transfer model for ozone profile retrieval using the analytical forward-adjoint perturbation theory approach," J. Geophys. Res. [Atmos.] **106,** 27291–27306 (2001).
33. O. P. Hasekamp, "Ozone profile retrieval from satellite measurements of backscattered sunlight," Ph.D. thesis (Free University of Amsterdam, 2002).
34. J. E. Hansen, "Multiple scattering of polarized light in planetary atmospheres. Part I. The doubling method," J. Atmos. Sci. **28,** 120–125 (1971).
35. B. M. Herman, W. Asous, and S. R. Browning, "A semi-analytic technique to integrate the radiative transfer equation over optical depth," J. Atmos. Sci. **37,** 1828–1838 (1980).
36. J. W. Hovenier, "Multiple scattering of polarized light in planetary atmospheres," Astron. Astrophys. **13,** 7–29 (1971).
37. G. P. Anderson, S. A. Clough, F. X. Kneizys, J. H. Chetwynd, and E. P. Shettle, *AFGL Atmospheric Constituent Profiles (0.120 km),* Report AFGL-TR-0208 (Environemental Research Papers, 1986).
38. T. Nakajima and M. Tanaka, "Algorithms for radiative intensity calculations in moderately thick atmospheres using a truncation approximation," J. Quant. Spectrosc. Radiat. Transfer **40,** 51–69 (1988).
39. M. I. Mishchenko, "The fast invariant imbedding method for polarized light—computational aspects and numerical results for Rayleigh scattering," J. Quant. Spectrosc. Radiat. Transfer **43,** 163–171 (1990).
40. M. D. King, "Number of terms required in the Fourier expansion of the reflection function for optically thick atmospheres," J. Quant. Spectrosc. Radiat. Transfer **30,** 143–161 (1983).
41. W. J. J. Knibbe, J. F. de Haan, J. W. Hovenier, D. M. Stam, R. B. A. Koelemeijer, and P. Stammes, "Deriving terrestrial cloud top pressure from photopolarimetry of reflected light," J. Quant. Spectrosc. Radiat. Transfer **64,** 173–199 (2000).
42. R. Bennartz and J. Fischer, "A modified *k*-distribution approach applied to narrow band water vapour and oxygen absorption estimates in the near infrared," J. Quant. Spectrosc. Radiat. Transfer **66,** 539–553 (2000).
43. M. Duan, Q. Min, and J. Li, "A fast radiative transfer model for simulating high-resolution absorption bands," J. Geophys. Res. **110,** D15201, doi:10.1029/2004JD005590 (2005).
44. L. S. Rothman, D. Jacquemart, A. Barbe, D. C. Benner, M. Birk, L. R. Brown, M. R. Carleer, C. Chackerian, K. Chance, L. H. Coudert, V. Dana, V. M. Devi, J. M. Flaud, R. R. Gamache, A. Goldman, J. M. Hartmann, K. W. Jucks, A. G. Maki, J. Y. Mandin, S. T. Massie, J. Orphal, A. Perrin, C. P. Rinsland, M. A. H. Smith, J. Tennyson, R. N. Tolchenov, R. A. Toth, J. Vander Auwera, P. Varanasi, and G. Wagner, "The HITRAN 2004 molecular spectroscopic database," J. Quant. Spectrosc. Radiat. Transfer **96,** 139–204 (2005).
45. O. Hasekamp and J. Landgraf, "Ozone profile retrieval from backscattered ultraviolet radiances: the inverse problem solved by regularization," J. Geophys. Res. [Atmos.] **106,** 8077–8088 (2001).
46. A. M. Bass and R. J. Paur, "The ultraviolet cross-sections of ozone. I. The measurements. II. Results and temperature dependence," in *Atmospheric Ozone: Proceedings of the Quadrennial* (D. Reidel, Dordrecht, The Netherlands, 1985), pp. 606–616.
47. O. P. Hasekamp, J. Landgraf, and R. van Oss, "The need of polarization modeling for ozone profile retrieval from backscattered sunlight," J. Geophys. Res. [Atmos.] **107,** doi:10.1029/2002JD002387 (2002).
48. B. van Diedenhoven, O. P. Hasekamp, and I. Aben, "Surface pressure retrieval from SCIAMACHY measurements in the O_2 A band: validation of the measurements and sensitivity on aerosols," Atmos. Chem. Phys. **5,** 2109–2120 (2005).
49. P. Stammes, J. F. de Haan, and J. W. Hovenier, "The polarized internal radiation field of a planetary atmosphere," Astron. Astrophys. **225,** 239–259 (1989).
50. O. P. Hasekamp and J. Landgraf, "Linearization of vector radiative transfer with respect to aerosol properties and its use in satellite remote sensing," J. Geophys. Res. **110,** D04203, doi:10.1029/2004JD005260 (2005).